Effect of impurities on the quantized conductance of narrow channels

C. S. Chu and R. S. Sorbello

Department of Physics and Laboratory for Surface Studies, University of Wisconsin-Milwaukee,
Milwaukee, Wisconsin 53201
(Received 13 February 1989)

The conductance G of narrow channels has been observed recently to be quantized in integer multiples of $2e^2/h$. We have calculated G for the case that an impurity is present in the channel. The channel is modeled as an electron waveguide, and the impurity is assumed to be an isotropic (s-like) scatterer. An analytic expression for G is obtained. We find that G is reduced below the unperturbed plateau values, and that for very strong scatterers the plateaus disappear. However, G exhibits two interesting features: First, G is pinned such that whenever the Fermi level is at the band bottom of the $(n+1)$th transverse subband $G = n(2e^2/h)$. Second, for attractive impurity potentials that have phase shift $\delta_0 \lesssim 30°$, the conductance is found to have a deep downward dip between adjacent conductance plateaus. We attribute these features to multiple scattering between the impurity and the waveguide walls.

I. INTRODUCTION

Electron transport in mesoscopic systems has recently attracted a great deal of attention[1,2] due to technological advances in the fabrication and characterization of submicrometer electron devices. The dimensions of these mesoscopic systems are smaller than the inelastic (incoherent) mean free path at sufficiently low temperatures, and as a consequence the electron wave functions can extend coherently over the entire system. Quantization effects will then occur when the dimensions of the system are comparable to the Fermi wavelength of the electrons. For purer systems, when the dimensions are smaller than the elastic (coherent) mean free path, the electron transport is in the ballistic regime and there is no scattering of any kind within the system.

The quantization effect in ballistic transport of electrons through mesoscopic systems has been studied in two recent experiments[3,4] using the split-gate technique.[5] The split gates form short constrictions that connect two larger areas of the two-dimensional electron gas (2DEG) in high-mobility GaAs-Al$_x$Ga$_{1-x}$As heterostructures. These constrictions are also known as Sharvin point contacts.[6] As the constriction width was made to increase by tuning the gate voltage, the measured conductance of the point contact was found to increase in integer multiples of $2e^2/h$. This novel quantized conductance phenomenon has since prompted a series of experimental[7,8] and theoretical[9-13] investigations. An early explanation[3] was suggested based upon electron transport through long and narrow channels, in which quantized conductance arises from the quantized transverse momentum inside the constriction. But the experimental situation involves only constrictions of finite length. Hence, questions still remain about the dependence of the conductance quantization on the geometry of the constriction, on the length and width of the constriction, on the effect of magnetic field, and on the disorder and tem-

perature in the constriction. In this paper, we shall focus our attention on the effects of disorder on the quantized conductance of narrow constrictions.

Theoretical studies have established some important features of the point-contact quantized conductance in the absence of disorder. We will now briefly mention these, restricting our attention to the case of zero magnetic field. For constrictions having abrupt openings, plateau features in the curve of conductance versus width occur for all constriction lengths, but these features become more obvious for longer constriction length and for smaller constriction width.[10-12] There are, in addition, resonance structures superposed on the plateaus in the conductance.[10-12] The origin of these resonance structures is the multiple scattering between the two ends of the constriction, and it occurs when the wave vector k of the electrons in one of the occupied subbands satisfies the condition kL is a multiple of π, where L is the constriction length. These resonances are artifacts of the assumed sharp edges at the end of the constrictions. A rounding of the constriction openings' sharp edges, with radius of curvature much greater than λ_F, results in removing the resonances.[9] Since the experimental results do not exhibit these resonances, the more appropriate theoretical model appears to be one in which the constriction openings are taken to be rounded, or gently flared,[9,14(a),14(b)] rather than abrupt. Numerical calculations of the potential profile of the constriction also support this view.[14(c)]

We therefore adopt the flared-horn aperture model[9,14(a)] for the constriction openings, where the radius of curvature is assumed to be much greater than λ_F. In this model, according to Glazman *et al.*[9] and Landauer,[14(a)] the transmission of the electrons through the constriction is adiabatic, i.e., the transverse energy level of the incident electron in the region far from the constriction evolves continuously into the transverse energy level of the transmitting wave function inside the constriction, with a one-to-one correspondence. If the

corresponding transverse energy level inside the constriction is lower than the electron energy, the electron will be almost completely transmitted through the constriction; otherwise, the electron will suffer nearly total reflection. Therefore, the left (right) going electron in the constriction is defined by the electrochemical potential deep inside the electron reservoir at the right- (left-) hand side of the constriction. The constriction region can then be modeled as an electron waveguide with well-defined incident electron distributions inside both ends of the waveguides.

In this paper, we study the effect of disorder on the quantized conductance by considering an impurity to be present inside the waveguide. Since in the actual experimental situation the electron mean free path is greater than the dimensions of the narrow channel, weak-disorder considerations are sufficient. The present model for an impurity in a narrow channel is similar to our recent model for an impurity in a thin film.[15] In our previous study the thin film was modeled as a planar waveguide; in the present study the narrow channel is modeled as a waveguide of finite cross section. Previously, we found that the residual resistivity due to an impurity in a thin film exhibits interesting features due to the multiple scattering of electrons between the impurity and the surfaces of the thin film. These features include resonancelike structures and a "transparency effect," which refers to a vanishing scattering cross section for the impurity. The transparency effect was found to occur when the film thickness is such that the Fermi level coincides with a subband minimum. By analogy, we expect similar effects to occur in narrow constrictions. This expectation is, in fact, borne out by the present work.

In our model, we take the cross section of the electron waveguide to be rectangular. The confined electrons have quantized transverse energy levels. To make contact with the 2DEG experimental systems, we consider the thickness of the waveguide to be so small that only the corresponding lowest quantized level plays a role. As the width of the waveguide is varied, the number of transverse levels below the Fermi level varies, leading to interesting structures in the conductance. We shall obtain the transmission matrix for our system by solving exactly the quantum-mechanical multiple scattering between the impurity and the electron waveguide, and we then relate the transmission matrix to the conductance.

The outline of this paper is as follows. In Sec. II we set up the quantum-mechanical multiple-scattering problem for an impurity inside the electron waveguide. Following Büttiker's approach[16,17] we derive the analytic expression for G, assuming a many-channel two-probe arrangement. The many channels in this case are the many occupied transverse subbands of the electron waveguide. In Sec. III we present some numerical examples to illustrate the variations of G with respect to the width of the electron waveguide. Finally, Sec. IV presents a discussion.

II. QUANTIZED CONDUCTANCE IN AN ELECTRON WAVEGUIDE

We consider an electron waveguide of rectangular cross section. Following Landauer's approach to conduc-

tance,[16,18] we connect the electron waveguide to electron reservoirs at each end. The electrochemical potential of the reservoir at the left- (right-) hand end is μ_1 (μ_2). To set up the transport of electrons within the waveguide, the electrochemical potentials μ_1 and μ_2 are shifted relatively in order to create a slight imbalance in the electron influx from both reservoirs. We then define $\mu_1 = \mu + \Delta\mu$ and $\mu_2 = \mu$, where $\Delta\mu > 0$. To find the transport current in the waveguide, we only have to consider those electrons which have energies E that are in the range $\mu < E < \mu + \Delta\mu$. These are the electrons that are incident from the left-hand side of the electron waveguide. For linear response $\Delta\mu \ll \mu$, and μ is the Fermi energy E_F of the electrons. In this section, we first study the scattering of each of these electrons within the waveguide in the presence of an impurity. We then find the total current in the waveguide, from which the conductance G is derived.

We choose a coordinate system for the electron waveguide such that the electrons are confined within the rectangular region $0 \le x \le d$ and $0 \le y \le W$, where d is the thickness and W the width. The electrons are free to move along L, the length of the waveguide, and the origin is located inside L. We let the excess incident electrons move along the $\hat{z}$ direction. The unperturbed electron states ψ^0_{mnk} in the waveguide have the form

$$\psi^0_{mnk}(\mathbf{r}) = \frac{2}{\sqrt{\Omega}} \sin\left[\frac{m\pi x}{d}\right] \sin\left[\frac{n\pi y}{W}\right] e^{ikz} , \qquad (1)$$

where m,n are positive integers signifying subband solutions, $k = (2\pi l)/L$ for integer l, and $\Omega = dWL$ is the waveguide volume. The electron states of Eq. (1) can be written as a superposition of four plane waves:

$$\psi^0_{mnk}(\mathbf{r}) = -\frac{1}{2\sqrt{\Omega}}(e^{i\mathbf{K}_{mn}^{++}\cdot\mathbf{r}} + e^{i\mathbf{K}_{mn}^{--}\cdot\mathbf{r}}$$

$$- e^{i\mathbf{K}_{mn}^{+-}\cdot\mathbf{r}} - e^{i\mathbf{K}_{mn}^{-+}\cdot\mathbf{r}})$$

$$= -\frac{1}{2\sqrt{\Omega}} \sum_{\alpha,\beta} \alpha\beta e^{i\mathbf{K}_{mn}^{\alpha\beta}\cdot\mathbf{r}} , \qquad (2a)$$

where $\alpha,\beta = (\pm)$ and

$$\mathbf{K}_{mn}^{\alpha\beta} = \alpha\left[\frac{m\pi}{d}\right]\hat{x} + \beta\left[\frac{n\pi}{W}\right]\hat{y} + k\hat{z} . \qquad (2b)$$

The energy of state ψ^0_{mnk} is $E_{mnk} = (\hbar^2 K^2/2m^*)$, where $K \equiv |\mathbf{K}_{mn}^{\alpha\beta}|$, and m^* is the effective mass of the electrons. Since we are interested only in the scattering of electrons at the Fermi energy E_F, the momentum k for an occupied subband (m,n) becomes k_{Fmn}, which satisfies the relation

$$E_F = \frac{\hbar^2 K_F^2}{2m^*} = \frac{\hbar^2}{2m^*}\left[\left[\frac{m\pi}{d}\right]^2 + \left[\frac{n\pi}{W}\right]^2 + k_{Fmn}^2\right] , \qquad (3)$$

and K becomes K_F. A subband (m,n) is occupied when $K_F^2 > (m\pi/d)^2 + (n\pi/W)^2$.

In this paper, we assume that $d \ll W$ and the Fermi level is sufficiently low that only subbands with $m = 1$ can be occupied. From now on, we simply let $m = 1$. An im-

purity is taken to lie within the waveguide and at the position $\mathbf{R}_0 = (d/2)\hat{\mathbf{x}} + b\hat{\mathbf{y}}$. Concerning the $\hat{\mathbf{x}}$ position of the impurity, we do not expect that the scattering is sensitive to the impurity position because the corresponding electron motion is frozen to the lowest subband. Furthermore, the choice that the impurity is located at the middle of the smallest confining dimension (thickness) simplifies the problem. The impurity potential is assumed to be spherically symmetric and confined within a small muffin-tin radius such that the impurity potential does not overlap with the waveguide's confining potential. The solution for the incident wave function scattered by the impurity in the electron waveguide is effectively the same as the solution for the four superposed propagating waves, as in Eq. (2a), incident upon a two-dimensional image-potential lattice in otherwise empty space. Of course, we use the image-problem solutions only within the region of the waveguide. The locations of the image potentials are given by

$$\mathbf{R}_{pj\nu} = \left[pd + \frac{d}{2}\right]\hat{\mathbf{x}} + (2jW + \nu b)\hat{\mathbf{y}} , \tag{4}$$

where p, j are integers labeling the unit cells of the image-potential plane, and $\nu = \pm 1$ denotes the two image potentials in a unit cell (see Fig. 1). A similar image-potential treatment has been applied to a thin-film geometry.[15] We remark that even though the electron motion along $\hat{\mathbf{x}}$ is taken to be frozen to the lowest subband, we allow, in our image potential treatment, the intermediate scattering processes of the electron to include virtual transitions to higher subbands. Our results thus contain the effect of finite thickness d. We now go on to outline the quantum-mechanical scattering problem.

A. Quantum-mechanical scattering problem

In this section, we consider the scattering of an incident electron state $\psi^0_{1nk_{F1n}}$ by the image-potential lattice
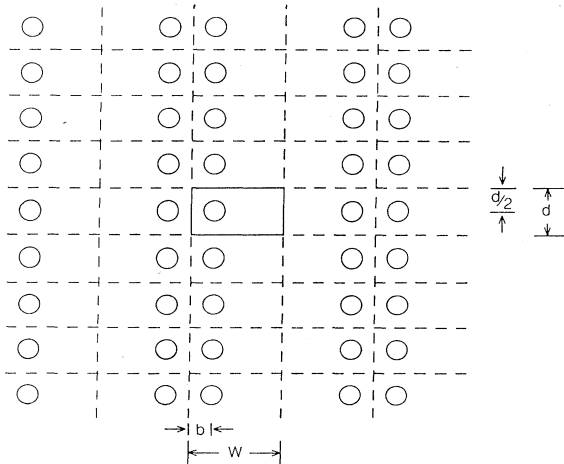
FIG. 1. Schematic diagram of an electron waveguide of rectangular cross section, an impurity inside the waveguide, and the two-dimensional image-potential lattice. The thickness of the waveguide is d, and its width is W.

plane. Steps to obtain the scattering state $\psi^{(+)}_{1nk_{F1n}}$ are outlined. The method is similar to standard techniques in low-energy electron diffraction (LEED) theory.[15,19] Since the image potential is spherically symmetric, it is convenient to expand the wave in spherical harmonics. To simplify notation we shall write $\psi^0_{1nk_{F1n}}$, $\psi^{(+)}_{1nk_{F1n}}$, and k_{F1n} as ψ^0_n, $\psi^{(+)}_n$, and k_{Fn}, respectively. From Eq. (2a), the expansion of the incident waves ψ^0_n with respect to $\mathbf{R}_{pj\nu}$ is given by

$$\psi^0_n(\mathbf{r}) = \sum_{L,M} a^{(0)}_{LM}(p,\nu)j_L(K_F|\mathbf{r} - \mathbf{R}_{pj\nu}|)$$
$$\times Y_{LM}[\hat{\Omega}(\mathbf{r} - \mathbf{R}_{pj\nu})] , \tag{5}$$

where

$$a^{(0)}_{LM}(p,\nu) = -\frac{2\pi}{\sqrt{\Omega}}i^L(-1)^p\sum_{\alpha,\beta}\alpha\beta i^\alpha e^{i\beta n\pi\nu b/W}$$
$$\times Y^*_{LM}[\hat{\mathbf{K}}^{\alpha\beta}_n] . \tag{6}$$

We note that $a^{(0)}_{LM}(p,\nu)$ is independent of j and it depends on p through the factor $(-1)^p$. From symmetry arguments, we deduce that after multiple scattering between the image potentials, the renormalized incident amplitude $a_{LM}(p,\nu)$ is still independent of j and it also depends on p through the $(-1)^p$ factor. We then define $a_{LM}(p,\nu) \equiv a_{LM}(\nu)(-1)^p$. The renormalized incident amplitude $a_{LM}(\nu)$ satisfies a self-consistency condition:[15,19]

$$a_{LM}(\nu) = a^{(0)}_{LM}(\nu) + i\sum'_{p,j,\nu'}(-1)^p$$
$$\times \sum_{L',M'}\sin\delta_{L'}e^{i\delta_{L'}}a_{L'M'}(\nu')$$
$$\times G_{L'M',LM}(\mathbf{R}_{00\nu} - \mathbf{R}_{pj\nu'}) , \tag{7}$$

where δ_L are the impurity scattering phase shifts. The prime on the summation indicates that the term which corresponds to $\mathbf{R}_{00\nu} = \mathbf{R}_{pj\nu'}$ is not included. From now on, we assume that the impurity scatters electrons isotropically (s-like scattering only). Using the fact that[19]

$$G_{00,00}(\mathbf{R}_{00\nu} - \mathbf{R}_{pj\nu'}) = h^{(1)}_0(K_F|\mathbf{R}_{00\nu} - \mathbf{R}_{pj\nu'}|) ,$$

Eq. (7) is simplified to

$$a_{00}(\nu) = a^{(0)}_{00}(\nu) + i\sum'_{pj\nu'}(-1)^p\sin\delta_0 e^{i\delta_0}a_{00}(\nu')$$
$$\times h^{(1)}_0(K_F|\mathbf{R}_{00\nu} - \mathbf{R}_{pj\nu'}|) , \tag{8}$$

where $h^{(1)}_0$ is the spherical Hankel function of the first kind.[20] The second term on the right-hand side of Eq. (8) is the wave incident upon one image potential due to the scattered waves from all other image potentials. The expression for $a^{(0)}_{00}(\nu)$ from Eq. (6) is given by

$$a^{(0)}_{00}(1) = 4\sqrt{\pi/\Omega}\sin\left[\frac{n\pi b}{W}\right] = -a^{(0)}_{00}(-1) . \tag{9}$$

Equation (8) is a matrix equation of order two and $a_{00}(\nu)$ is solved to give

$$a_{00}(1) = \frac{4\sqrt{\pi/\Omega}\sin\left[\dfrac{n\pi b}{W}\right]}{1 - i\sin\delta_0 e^{i\delta_0}[\chi(1,1) - \chi(1,-1)]}$$

$$= -a_{00}(-1) , \tag{10}$$

where

$$\chi(1,1) = \sum_{p,j}{}' (-1)^p h_0^{(1)}(K_F|\mathbf{R}_{001} - \mathbf{R}_{pj,1}|) \tag{11a}$$

and

$$\chi(1,-1) = \sum_{p,j} (-1)^p h_0^{(1)}(K_F|\mathbf{R}_{001} - \mathbf{R}_{pj,-1}|) . \tag{11b}$$

Again the sum in Eq. (11a) does not include the term which corresponds to $\mathbf{R}_{001} = \mathbf{R}_{pj,1}$.

The total scattered wave ϕ_n^{scatt} is given by

$$\phi_n^{\text{scatt}}(\mathbf{r}) = \frac{i\sin\delta_0 e^{i\delta_0}}{\sqrt{4\pi}} \sum_\nu a_{00}(\nu) \sum_{p,j}$$

$$\times (-1)^p h_0^{(1)}(K_F|\mathbf{r} - \mathbf{R}_{pj\nu}|) . \tag{12}$$

Using the Poisson sum formula,[15,21] we convert the lattice sum in Eq. (12) into a convenient form:

$$\sum_{p,j} (-1)^p h_0^{(1)}(K_F|\mathbf{r} - \mathbf{R}_{pj\nu}|) = \frac{2\pi}{WK_Fd} \sum_{\substack{l\geq 1\\(\text{odd})}} \sin\left[\frac{l\pi}{2}\right]\sin\left[\frac{l\pi x}{d}\right]$$

$$\times \sum_{n'} \frac{\exp\left\{i\left[K_F^2 - \left[\dfrac{l\pi}{d}\right]^2 - \left[\dfrac{n'\pi}{W}\right]^2\right]^{1/2}|z|\right\}}{\left[K_F^2 - \left[\dfrac{l\pi}{d}\right]^2 - \left[\dfrac{n'\pi}{W}\right]^2\right]^{1/2}} e^{i(n'\pi/W)(\nu b - y)} , \tag{13}$$

where the square root takes on the branch $\sqrt{-|x|} = i\sqrt{|x|}$. There are exponentially decaying factors in the sum of Eq. (13) for terms that correspond to $K_F^2 < (l\pi/d)^2 + (n'\pi/W)^2$. In this case we have assumed $\pi/d < K_F < 2\pi/d$, and if we are interested only in regions $|z| > d$, we can therefore neglect all the $l > 1$ terms in Eq. (13). The total scattered wave is then simplified to

$$\phi_n^{\text{scatt}}(\mathbf{r}) = \frac{16\pi}{\sqrt{\Omega}} \frac{\sin\left[\dfrac{n\pi b}{W}\right]\sin\left[\dfrac{\pi x}{d}\right]}{WK_Fd} \frac{i\sin\delta_0 e^{i\delta_0}}{1 - i\sin\delta_0 e^{i\delta_0}[\chi(1,1) - \chi(1,-1)]}$$

$$\times \sum_{n'\geq 1} \frac{\exp\left\{i\left[K_F^2 - \left[\dfrac{\pi}{d}\right]^2 - \left[\dfrac{n'\pi}{W}\right]^2\right]^{1/2}|z|\right\}}{\left[K_F^2 - \left[\dfrac{\pi}{d}\right]^2 - \left[\dfrac{n'\pi}{W}\right]^2\right]^{1/2}} \sin\left[\frac{n'\pi b}{W}\right]\sin\left[\frac{n'\pi y}{W}\right] . \tag{14}$$

The scattering state is given by

$$\psi_n^{(+)}(\mathbf{r}) = \psi_n^0(\mathbf{r}) + \phi_n^{\text{scatt}}(\mathbf{r}) . \tag{15}$$

B. Conductance in electron waveguides

In this section we first find the transmitted current in the electron waveguide for an incident state ψ_n^0. Then, using the Landauer picture[16,18] in which the incident electron distribution is specified by the two reservoirs connected to the waveguide, we find the total transmitted current. The potential difference, measured between two points deep inside both reservoirs, is essentially the electrochemical potential difference between the reservoirs. Hence we derive the conductance G, which is the ratio of the total transmitted current to the potential difference.

The transmission matrix $t_{nn'}$ is defined as follows:

$$\psi_n^{(+)}(\mathbf{r}) = \sum_{n'\geq 1} t_{nn'}\psi_{n'}^0(\mathbf{r}) , \tag{16}$$

in the region $z > 0$, and $k_{Fn'}$, the effective Fermi wave vector for subband $(1, n')$, is given by

$$k_{Fn'} = \begin{cases} \left\{ \left[K_F^2 - \left[\dfrac{\pi}{d} \right]^2 - \left[\dfrac{n'\pi}{W} \right]^2 \right] \right\}^{1/2} & \text{for } K_F^2 > \left[\dfrac{\pi}{d} \right]^2 + \left[\dfrac{n'\pi}{W} \right]^2 \\[2ex] i \left[\left[\dfrac{\pi}{d} \right]^2 + \left[\dfrac{n'\pi}{W} \right]^2 - K_F^2 \right]^{1/2} & \text{for } K_F^2 < \left[\dfrac{\pi}{d} \right]^2 + \left[\dfrac{n'\pi}{W} \right]^2 . \end{cases}$$

From Eqs. (1), (14), (15), and (16), we obtain the expression for $t_{nn'}$ which is given by

$$t_{nn'} = \frac{8\pi}{WK_Fd} \frac{\sin\left[\dfrac{n\pi b}{W} \right] \sin\left[\dfrac{n'\pi b}{W} \right]}{k_{Fn'}} \left[\frac{e^{-i\delta_0}}{i\sin\delta_0} - \chi(1,1) + \chi(1,-1) \right]^{-1} + \delta_{nn'} . \tag{17}$$

The first term on the right-hand side of Eq. (17) is the channel-mixing term that allows the electrons to scatter from one subband to other subbands. Perfect waveguide results are obtained by dropping this channel-mixing term.

Corresponding to the incident state ψ_n^0, the transmitted current along the waveguide is

$$i_n = -\frac{e\hbar}{m^*} \int dx\, dy\, \text{Re}\left[\frac{1}{i} \psi_n^{(+)*} \frac{\partial}{\partial z} \psi_n^{(+)} \right]$$

$$= -\frac{ev_{Fn}}{L} \sum_{n'=1}^{N} t_{nn'}^* t_{nn'} \frac{k_{Fn'}}{k_{Fn}} , \tag{18}$$

where N is the total number of occupied subbands, e is the magnitude of the electron charge, and $v_{Fn} = (\hbar k_{Fn}/m^*)$ is the effective Fermi velocity for subband $(1,n)$. The total transmitted current I_{tran} is given by

$$I_{\text{tran}} = \sum_{n=1}^{N} i_n \left[\frac{\partial N}{\partial \epsilon} \right]_n (\mu_1 - \mu_2) , \tag{19}$$

where

$$\left[\frac{\partial N}{\partial \epsilon} \right]_n = \frac{L}{\pi \hbar v_{Fn}}$$

is the density of states for subband $(1,n)$ including only states of positive $\hat{z}$ momentum and both spin states. The potential difference δV for two points deep inside both reservoirs is $\mu_1 - \mu_2 = -e\delta V$. Therefore, the conductance G is given by

$$G = \frac{I_{\text{tran}}}{\delta V} = \frac{e^2}{\pi \hbar} \sum_{n=1}^{N} \sum_{n'=1}^{N} t_{nn'}^* t_{nn'} \frac{k_{Fn'}}{k_{Fn}} , \tag{20}$$

which is the many-channel expression for two-probe conductance.[22] As we have pointed out earlier, the vanishing of the channel-mixing feature in the transmission matrix leads via Eq. (20) to $G = (Ne^2/\pi\hbar)$ which is the result for a perfect electron waveguide. This limit obviously can be achieved by letting δ_0 go to zero. However, even for finite δ_0, it is still possible for the channel-mixing term to vanish. This turns out to be a consequence of the multiple scattering between the impurity and the electron waveguide. In the following we rewrite Eq. (20) into a form such that the aforementioned feature of G becomes apparent. Substituting the expression of $t_{nn'}$ into Eq. (20), we obtain

$$G = \frac{e^2}{\pi \hbar} \left[N - \frac{\beta^2}{\left| \dfrac{e^{-i\delta_0}}{i\sin\delta_0} - \chi(1,1) + \chi(1,-1) \right|^2} \right] , \tag{21}$$

where

$$\beta = \frac{8\pi}{WK_Fd} \sum_{n=1}^{N} \frac{\sin^2\left[\dfrac{n\pi b}{W} \right]}{k_{Fn}} . \tag{22}$$

Furthermore, the real part of the lattice sums in $\chi(1,1)$ and $\chi(1,-1)$ can be simplified (see Appendix) to give the following identity:

$$\text{Re}\left[\frac{e^{-i\delta_0}}{i\sin\delta_0} - \chi(1,1) + \chi(1,-1) \right] = -\beta . \tag{23}$$

The imaginary part of the lattice sums in $\chi(1,1)$ and $\chi(1,-1)$ can be converted from double sum to single sum; the expressions are given in the Appendix also. Finally, the conductance G given by Eq. (21) can be written in the form

$$G = \frac{e^2}{\pi \hbar} \left[N - \frac{\beta^2}{\beta^2 + \{\cot\delta_0 + \text{Im}[\chi(1,1) - \chi(1,-1)]\}^2} \right] . \tag{24}$$

The first term in Eq. (24) is the conductance of a perfect electron waveguide, whereas the second term is the correction due to the presence of an impurity. We note, from the analysis in the Appendix, that if the Fermi level is just below the $(N+1)$th subband, the expression $\text{Im}[\chi(1,1) - \chi(1,-1)]$ becomes very large and negative. Hence the correction term due to the impurity is very small and $G \simeq (Ne^2/\pi\hbar)$ in this case. The impurity has no effect on the conductance under this particular condition. Evidently, this interesting transparency effect is a consequence of multiple scattering between the impurity and the waveguide walls. We also note, from Eq. (24), that when the condition

$$\cot\delta_0 + \text{Im}[\chi(1,1) - \chi(1,-1)] = 0$$

is satisfied, the conductance G will exhibit a downward dip structure and the conductance at the dip position will be $G = [(N-1)e^2/\pi\hbar]$. In contrast with the above features, we compare the Born approximation limit of Eq. (24), given by

$$G = \frac{e^2}{\pi\hbar}[N - (\beta\delta_0)^2] . \tag{25}$$

Equation (25) gives an unphysical result that G tends to very large negative values when the Fermi level is above and close to a subband bottom. Therefore multiple-scattering considerations are necessary even for weak scatterers.

III. NUMERICAL RESULTS

We will demonstrate here numerically the features of G that we have mentioned in the last section. The physical parameters we choose are characteristic of the high-mobility GaAs-Al$_x$Ga$_{1-x}$As heterostructure that has been used for the quantized conductance experiments.[3,4] The thickness d of the two-dimensional electron gas layer is chosen to be 100 Å. The electron density is chosen to be $2.51 \times 10^{11}/\text{cm}^2$. Hence the corresponding two-dimensional Fermi wave vector λ_F is 500 Å and remains fixed at this value as we allow the width W of the con-

striction to vary. For definiteness we take the y coordinate of the impurity to be at a distance of 50 Å from the center of the channel.[23]

In Fig. 2 we present a plot of the conductance G versus the width W for the phase shift $\delta_0 = 30°$. This curve shows the features of G for the case of a weak scatterer. The features of G for the case of a strong scatterer are shown in Fig. 3 where δ_0 is chosen to be 60° and 90°. Repulsive potential results are shown in Fig. 4, where $\delta_0 = -30°$ and $-60°$ conductance curves are plotted. For the purpose of comparison, the perfect-constriction result is also plotted in all the three figures and is indicated by the dashed curve. From these curves we observe that the conductance is, in general, lowered due to the presence of an impurity. In the case of the weak scatterer ($\delta_0 \lesssim 30°$), the plateau structures are essentially intact even though the plateaus are reduced below the unperturbed values. However, in the case of the strong scatterer, the plateaus disappear. The two novel features which we have previously mentioned are visible in our figures. First, G is pinned such that whenever the Fermi level is at the band bottom of the $(n+1)$th transverse subband, $G = n(2e^2/\hbar)$. This feature does not depend on the strength of the scatterer. Second, for attractive impurity potentials that are not too strong ($0 < \delta_0 \lesssim 30°$), the conductance G exhibits a downward dip between plateaus.[24] The weaker the scatterer, the sharper will be the downward dip and the closer the dip position will be to W
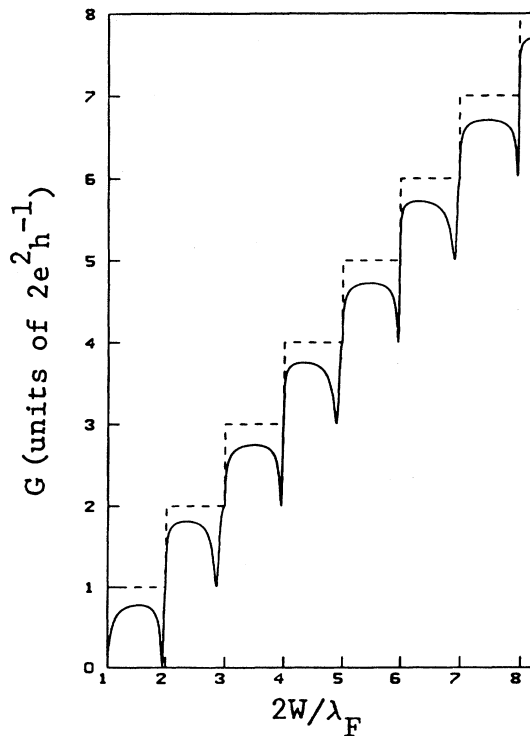
FIG. 2. Conductance G for an electron waveguide plotted as a function of the width W of the channel. The curve is for an attractive weak-scattering impurity with phase shift $\delta_0 = 30°$. The perfect waveguide result is indicated by the dashed steps.
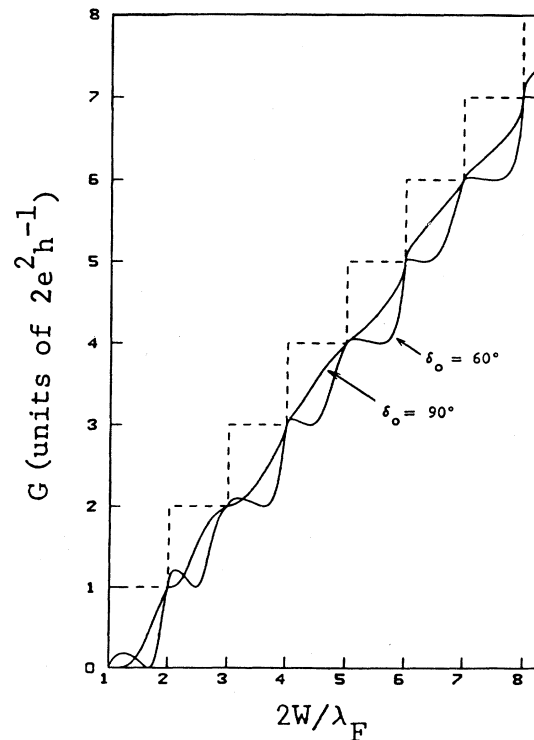
FIG. 3. Conductance G vs W for attractive strong-scattering impurities. The phase shifts are $\delta_0 = 60°$ and $\delta_0 = 90°$. The perfect waveguide result is indicated by the dashed steps.
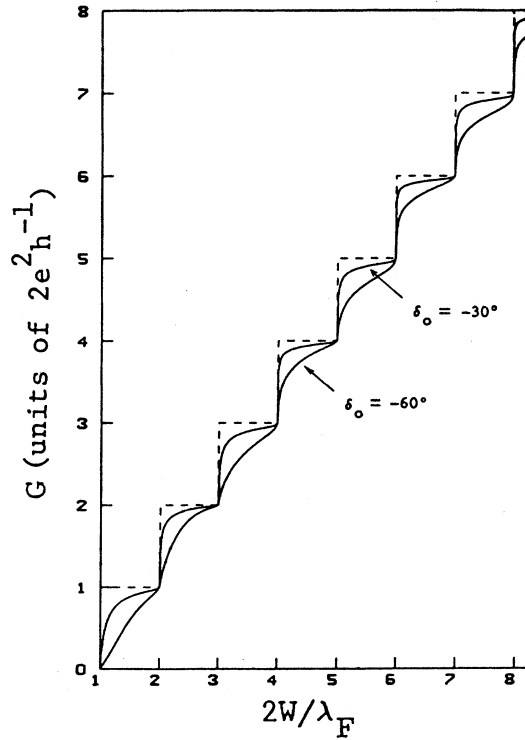
FIG. 4. Conductance G vs W for repulsive impurities. The phase shifts are $\delta_0 = -30°$ and $\delta_0 = -60°$. The perfect waveguide result is indicated by the dashed steps.

values where the Fermi level is at a subband bottom. The remnants of these downward dips can still be seen in the stronger scatterer case where $\delta_0 = 60°$. Actually, it is the widening of the downward dips in the stronger scatterer case that destroys the plateaus. However, this downward-dip feature does not appear in the repulsive scatterer case.

IV. DISCUSSION

A wave propagation analysis has been applied to study the effect of an impurity on the conductance of a narrow channel. We find that, in general, the conductance is lowered due to the presence of an impurity. Our findings also indicate that the plateau structures in the conductance, though able to survive in the presence of a weak scatterer, are essentially destroyed by a strong scatterer. Furthermore, for isotropic scatterers (s-like scattering only), we find two new features. First, G equals $n(2e^2/h)$ whenever the Fermi level is at the band bottom of the $(n+1)$th subband, irrespective of the strength of the scatterer. Second, G exhibits downward dips with one dip between every neighboring plateau for attractive and weak $(0 < \delta_0 \lesssim 30°)$ impurity potentials. These two features are consequences of multiple scattering between the impurity and the constriction.

We point out that there is a direct relationship between the pinned feature of G, when the Fermi level is at a subband bottom, and the divergences in the lattice sums

$\chi(1,1)$ and $\chi(1,-1)$. In solving the multiple scattering between the impurity and all of its image potentials, the lattice sums appear in the denominator of the subband mixing terms in the conductance. The divergences of these sums lead to the vanishing of the subband mixing term and hence to the pinned feature of G. Similarly we expect, in the case of more than one impurity, that the lattice sums would also enter a determinant which would form the denominator of the subband mixing term. Therefore we expect the pinned feature of G to be valid even for many s scatterers inside the constriction.

We have assumed, in this study, that the impurity is an s-like scatterer. It is, therefore, relevant to ask whether our results can hold beyond this assumption. An analysis for an impurity which is both an s and p scatter is being carried out,[25] and we find that when the Fermi level is at the $(n+1)$th subband bottom and the phase shift $\delta_1 \lesssim 30°$, the conductance $G \simeq (n-\Delta)(2e^2/h)$, where $\Delta \lesssim 0.10$. This implies that the pinned feature of G is not completely lost beyond s-scatterer analysis. It also seems that this feature of G can allow us to see how dominant is the s component in the scattering properties of the impurity. Since the physical dimensions of the constriction used in our numerical examples are within present experimental attainability, it is hoped that our work will encourage further experimental effort on the effects of impurities on the quantized conductance of a narrow constriction.

ACKNOWLEDGMENTS

APPENDIX

In this Appendix we briefly outline the calculation of the lattice sums $\chi(1,1)$ and $\chi(1,-1)$. The lattice sum $\chi(1,1)$ in Eq. (11a) can be written in the form

$$\chi(1,1) = {\sum_p}' (-1)^p h_0^{(1)}(Kd|p|)$$
$$+ {\sum_j}' \sum_p (-1)^p h_0^{(1)}(K\sqrt{p^2 d^2 + 4j^2 W^2}) , \qquad \text{(A1)}$$

where $K \equiv K_F$, and the primes signify that the summation index is not zero. The first term in the right-hand side of Eq. (A1) becomes

$${\sum_p}' (-1)^p h_0^{(1)}(Kd|p|) \equiv \frac{1}{i}(A_0 - B_0) , \qquad \text{(A2)}$$

where

$$A_0 \equiv \frac{1}{Kd} \sum_{j=1}^{\infty} \frac{e^{2iKdj}}{j} , \qquad \text{(A3)}$$

and

$$B_0 \equiv \frac{1}{2Kd} \sum_{j=-\infty}^{\infty} \frac{e^{2iKd|j-1/2|}}{|j-1/2|} . \qquad \text{(A4)}$$

The sum A_0 can be performed analytically,[26] and the result is

$$A_0 = \frac{1}{2kd}\left[\ln\frac{1}{2(1-\cos x)}+i(\pi-x)\right], \quad \text{(A5)}$$

where $x = 2Kd - 2\pi I$ and I is the largest integer smaller than (Kd/π). Similarly, the sum B_0 can be shown to be of the form

$$B_0 = \frac{1}{2Kd}\sum_{j=-\infty}^{\infty}\frac{\cos(2Kd|j-\frac{1}{2}|)}{|j-\frac{1}{2}|}$$

$$+\frac{i\pi}{2Kd}\left[1+2\sum_{\nu=1}^{I}\cos(\pi\nu)\right]. \quad \text{(A6)}$$

We note that in this paper we are in the regime $1 < (Kd/\pi) < 2$ and so I is simply equal to one.

The second term in the right-hand side of Eq. (A1) can be written as

$$\frac{\pi}{Kd}\sum_j{}'\sum_l H_0^{(1)}[2W|j|\sqrt{K^2-(\pi/d)^2(2l-1)^2}],$$

where the sum over p is replaced by a sum over l using the Poisson sum formula.[21] Both p and l are integers. But in this paper, we are in the small-d regime so that the terms other than $l = 0, 1$ in the above sum are exponentially small and can be neglected. Therefore we have

$$\chi(1,1) \simeq \frac{1}{i}(A_0 - B_0)$$

$$+\frac{4\pi}{Kd}\sum_{j=1}^{\infty}J_0[2jW\sqrt{K^2-(\pi/d)^2}]$$

$$+i\frac{4\pi}{Kd}\sum_{j=1}^{\infty}N_0[2jW\sqrt{K^2-(\pi/d)^2}]. \quad \text{(A7)}$$

We note that the real part of the right-hand side in Eq. (A7) is the exact real part of the lattice sum $\chi(1,1)$. The two sums in Eq. (A7) can be converted to the form[27]

$$\sum_{j=1}^{\infty}J_0[j\xi] = -\frac{1}{2}+\frac{1}{\xi}+2\sum_{m=1}^{N}\frac{1}{\sqrt{\xi^2-4m^2\pi^2}}, \quad \text{(A8)}$$

and

$$\sum_{j=1}^{\infty}N_0[j\xi] = -\frac{1}{\pi}\left[C+\ln\frac{\xi}{4\pi}\right]+\frac{1}{\pi}\sum_{l=1}^{N}\frac{1}{l}$$

$$-2\sum_{l=N+1}^{\infty}\left[\frac{1}{\sqrt{(2\pi l)^2-\xi^2}}-\frac{1}{2\pi l}\right], \quad \text{(A9)}$$

where $\xi = 2W\sqrt{K^2-(\pi/d)^2}$ and $2\pi N < \xi < 2(N+1)\pi$. Here C is the Euler constant.

For the lattice sum $\chi(1,-1)$ in Eq. (11b), we have

$$\chi(1,-1) = \sum_{p,j}(-1)^p h_0^{(1)}[K\sqrt{p^2d^2+(2jW+2b)^2}],$$

which can be written in the form

$$\chi(1,-1) = \frac{2\pi}{Kd}\sum_{\substack{l=1\\(\text{odd }l)}}^{\infty}\sum_j H_0^{(1)}[\,|2jW+2b|$$

$$\times\sqrt{K^2-(\pi l/d)^2}\,], \quad \text{(A10)}$$

using again the Poisson formula.[21] Within our small-d regime, we only need to keep the $j = 0$ term in Eq. (A10) when $l \geq 3$. We apply the Poisson sum formula to summation over j and obtain

$$\chi(1,-1) \simeq -\frac{4i}{Kd}\sum_{\substack{l=3\\(\text{odd }l)}}^{\infty}[K_0\sqrt{2b(\pi l/d)^2-K^2}]$$

$$+\frac{2\pi}{KdW}\sum_m\frac{e^{i2bm\pi/W}}{\sqrt{K^2-(\pi/d)^2-(m\pi/W)^2}}. \quad \text{(A11)}$$

Again, we note that the real part of $\chi(1,-1)$ in Eq. (A11) is the exact result. Putting together Eqs. (A7), (A5), (A6), (A8), (A9), and (A11), we can establish the identity

$$\text{Re}\left[\frac{e^{-i\delta_0}}{i\sin\delta_0}-\chi(1,1)+\chi(1,-1)\right] = -\beta. \quad \text{(A12)}$$

The behavior of the lattice sums $\chi(1,1)$ and $\chi(1,-1)$ is more apparent in Eqs. (A7) and (A11). If the Fermi level is just above a subband bottom, $2\pi(N+1) > \xi \gtrsim 2\pi N$, and the real parts of $\chi(1,1)$ and $\chi(1,-1)$ become very large. On the other hand, if the Fermi level is just below a subband bottom $2\pi(N+1) \gtrsim \xi > 2\pi N$, and the imaginary parts of $\chi(1,1)$ and $\chi(1,-1)$ become very large. From our numerical calculations we also find that $\text{Im}[\chi(1,1)-\chi(1,-1)]$ becomes large and negative as the Fermi level is approaching the subband bottom of an unoccupied subband.

[1]See, for example, IBM J. Res. Dev. **32**, 304 (1988).

[2]Y. Imry, in *Directions in Condensed Matter Physics*, edited by G. Grinstein and G. Mazenko (World Scientific, Singapore, 1986), Vol. 1, p. 102.

[3]B. J. van Wees, H. van Houten, C. W. J. Beenakker, J. G. Williamson, L. P. Kouwenhoven, D. van der Marel, and C. T. Foxon, Phys. Rev. Lett. **60**, 848 (1988).

[4]D. A. Wharam, T. J. Thornton, R. Newbury, M. Pepper, H. Ahmed, J. E. F. Frost, D. G. Hasko, D. C. Peacock, D. A. Ritchie, and G. A. C. Jones, J. Phys. C **21**, L209 (1988).

[5]T. J. Thornton, M. Pepper, H. Ahmed, D. Andrews, and G. J. Davies, Phys. Rev. Lett. **56**, 1198 (1986).

[6]Yu. V. Sharvin, Zh. Eksp. Teor. Fiz. **48**, 984 (1965) [Sov. Phys.—JETP **21**, 655 (1965)].

[7]D. A. Wharam, M. Pepper, H. Ahmed, J. E. F. Frost, D. G. Hasko, D. C. Peacock, D. A. Ritchie, and G. A. C. Jones, J. Phys. C **21**, L887 (1988).

[8]C. G. Smith, M. Pepper, H. Ahmed, J. E. F. Frost, D. G. Hasko, D. C. Peacock, D. A. Ritchie, and G. A. C. Jones, J. Phys. C **21**, L893 (1988).

[9]L. I. Glazman, G. B. Lesovick, D. E. Khmelnitskii, and R. E. Shekhter, Pisma Zh. Eksp. Teor. Fiz. **48**, 218 (1988) [JETP Lett. **48**, 238 (1988)].

[10]G. Kirczenow, Solid State Commun. **68**, 715 (1988).

[11]A. Szafer and A. D. Stone, Phys. Rev. Lett. **62**, 300 (1989).

[12]E. G. Haanappel and D. van der Marel, Phys. Rev. B **39**, 7811

(1989).

[13]J. Masek and B. Kramer (unpublsihed).

[14](a) R. Landauer, Z. Phys. B **68**, 217 (1987); (b) R. Landauer (unpublished) has given further considerations of the effect of aperture geometry and voltage-probe placement; (c) A. Kumar, S. E. Laux, and F. Stern, Bull. Am. Phys. Soc. **34**, 589 (1989).

[15]C. S. Chu and R. S. Sorbello, Phys. Rev. B **38**, 7260 (1988).

[16]M. Büttiker, IBM J. Res. Dev. **32**, 317 (1988).

[17]M. Büttiker, Phys. Rev. B **38**, 9375 (1988).

[18]M. Büttiker, Y. Imry, R. Landauer, and S. Pinhas, Phys. Rev. B **31**, 6207 (1985).

[19]J. B. Pendry, *Low-Energy Electron Diffraction Theory* (Academic, London, 1974).

[20]All spherical and cylindrical special functions are defined the same way as in the book by J. D. Jackson, *Classical Electrodynamics* (Wiley, New York, 1975).

[21]See, for example, P. M. Morse and H. Feshbach, *Methods of Theoretical Physics* (McGraw-Hill, New York, 1953), p. 467.

[22]The conductance expression in Eq. (20) is equivalent to that given by Büttiker in Ref. 17. But note that our $t_{nn'}$ is defined differently from his.

[23]Our choice of 50 Å for the distance of the impurity from the center of the channel assures that the impurity is away from those special points where the wave function of the highest occupied subband has nodes. When the Fermi level is at the bottom of a subband, these nodes occur at positions where $|y - \frac{1}{2}W| = \frac{1}{2}\lambda_F(s + \frac{1}{2})$ or $s\lambda_F/2$, where $s = 0, 1, 2, \ldots$. When the impurity is at one of these nodes β is finite, whereas for all other impurity positions β is infinite at that Fermi level. The qualitative change in Fig. 2 when the impurity is at one of these nodes is that alternate downward dips are removed, namely those dips occurring in the immediate vicinity of those W values corresponding to the onset of a new subband and for which the impurity is at a node of the transverse wave function of the new subband. Thus, for example, when the impurity is at the center of the channel ($y = W/2$), the downward dips in Fig. 2 which are in the vicinity of $2W/\lambda_F = 2, 4, 6, \ldots$ are removed.

[24]After completion of our work, we received a copy of work done by J. Masek and B. Kramer (unpublished) in which qualitatively similar behavior for the conductance is obtained within an Anderson model.

[25]C. S. Chu and R. S. Sorbello (unpublished).

[26]See, for example, I. S. Gradshteyn and I. M. Ryzhik, *Table of Integrals, Series, and Products* (Academic, Orlando, 1983), p. 38.

[27]See Ref. 26, pp. 976 and 977.